# Blast Resilience Enhancement of Cable-Supported Façade Utilizing Super-Elastic Shape Memory Alloy

**Shashank Gupta[1*], Euan Stoddart[2], Andrew Morrison[2]**

* Corresponding author
1 University of Wolverhampton, School of Architecture and Built Environment, UK, shashank.gupta@wlv.ac.uk
2 Thornton Tomasetti, UK

## Abstract

*Due to an increased level of threat, the design of buildings to resist blast loads has gained importance. The most vulnerable component of the building is typically the cladding system, generally being lightweight and directly facing the hazard with large, exposed surface areas. A large number of cladding materials are available, with architectural intent constantly driving the development of new products and systems. Glazed façades are aesthetically appealing and are popular among architects. In this paper, the use of super-elastic shape memory alloy (SMA) to improve the blast resilience of a cable-supported system is explored. The critical component of these systems is the high strength steel material cable. In the present study it is rendered hybrid (Steel-SMA), by attaching SMA cable(s) to the steel cable at one or both ends, and the dynamic performance under blast is studied. It is shown that the introduction of SMA in the cable has the potential to improve the resilience of the façade system.*

## Keywords

*Shape memory alloys, glazed façades, cable supported façades, SMA cables, blast resilient design*

10.7480/jfde.2021.2.5331

# 1 INTRODUCTION

Over the last few decades, considerable attention has been focused on the behaviour of engineered structures under extreme loads such as blast, fire, and impact. The design of buildings to resist blast loads has gained particular attention due to the high levels of damage observed from numerous examples of terrorist activities. The attack on Murrah Federal Building in Oklahoma City in 1995 is an example in which a large vehicle-borne improvised device (VBIED) was detonated from a small standoff. The blast resulted in the partial collapse of the building, which led to amendments to the US codes to improve robustness in federal buildings (Cormie et al., 2009). The blast at Bishopgate in 1993 resulted in widespread breakage of windows, generating a significant internal hazard. The windows mostly had annealed glass, which shattered, generating lot of debris. Casualties from such an event occur not only as a consequence of the direct blast effects, but also due to the associated structural failures that result in local or global collapse of the structure. The Centre for the Protection of National Infrastructure (CPNI), the government authority for protective security advice to the UK national infrastructure, states: "Up to 95% of all injuries from bomb blast are caused by flying or falling glass."

Blast/explosive loading results in high pressures on building façades and subsequent large demands on the fixings. The glazed façade is typically designed using laminated glass, which is able to fracture but maintains its integrity due to a flexible interlayer which holds the fragments together and therefore generation of internal debris is minimised. Whilst damage to the glazing is typically allowed within the performance criteria, it is generally specified that the façade must remain attached to the main structure during and following an event so that it does not present an additional hazard or block ingress/egress routes. Hence, the fixings are a critical component of the design in order to maintain structural integrity of the façade system and ensure it remains attached. The dynamic reactions generated at the fixings are a function of the stiffness of the system. Based on the requirement to maintain integrity following an explosion event, the fixings are typically designed for strength and hence do not allow much deflection or energy absorption.

Blast-resistant glazed façades are designed using single or multi-degree of freedom models as well as by finite element analysis (FEA). Zobec et al. (2018) present an innovative design tool for the optimisation of blast-enhanced façade systems. They discuss the single degree of freedom (SDOF) approach in conjunction with FEA as a means to analyse the design of the façade systems. They conclude that a balance between the blast energy dissipation and glass fragmentation is required. A novel fragmentation tool is proposed for the design, which shows excellent correlation with blast arena tests. Cormie et al. (2009) discuss the blast effects on buildings and provide several approaches for designing glazed as well as other types of façades. Morison (2007; 2013) analysed the resistance of laminated glass to blast pressure using the SDOF model. The thesis (Morison, 2007) was based on a number of experiments, which enabled characterisation of the glass behaviour under blast. Gupta et al. (2018b) present a review of the dynamic behaviour of various types of cladding systems subjected to blast loading. Pressure-Impulse (PI) curves used to evaluate the response against a range of explosion hazards were developed for critical structural elements. Bedon et al. (2018) have presented a comprehensive review of the state-of-the-art analysis and design methods used for glass façades that are subjected to extreme loads.

Planar glazing is increasingly used for commercial buildings where architects want to reduce the visual impact of any support systems. These employ corner connections, sometimes referred to as spider fixings, rather than conventional mullions and transoms to support the glazing. The cable-supported façade systems are aesthetically appealing due to high transparency as compared to other

glazed façade systems. The most common layout consists of pre-stressed cables that span vertically between lower- and upper-level floor slabs. The cables are spaced at approximately the width of the glass panel and cables are stiffened by pre-stressing, which enables them to carry all loads transmitted from the glass façade. Cable-supported façades have been utilised on many buildings, for example, the lobby of a 53-storey tower at South Wacker (Chicago), façade of Lufthansa Aviation Centre and Alice Tully Hall, Lincoln Centre, Manhattan (Yussof, 2015). Whilst these systems are able to be used for normal design conditions, when the façade is subject to extreme loads such as blast, the support reactions and cable stresses can be excessive. Thus, the connection of the cable to the structure and the cables themselves require detailed consideration to ensure the structural integrity of the system and prevent collapse of the façade.

The behaviour of cables and the cable connections in such systems has been the subject of recent research. Amadio and Bedon (2012a) considered an elasto-plastic (friction energy) dissipative device for the mitigation of hazards of the blast-resisting cable-supported glazing façade. In another publication (2012b), they developed the design of the spider connector with an in-built viscoelastic damper, and theoretically analysed its effectiveness. The combined effect of viscoelastic and friction-energy-dissipating devices applied to a cable net façade was studied by Bedon and Amadio (2014). To incorporate these energy-dissipating devices in the façade, an outline of design procedure was also presented. Dos Santos et al. (2016b) conducted analysis using a lumped parameter FE model and proposed an active control system using a proportional-integral-derivative (PID) controller to limit tension in cable and stresses in glass panes. Piyasena et al. (2019) have shown that in comparison to the cable net façade, cable truss façades have reduced deflections but larger cable forces. More recently, Royer-Carfagni and Viviani (2020) performed a non-linear dynamic analysis of a cable façade using a simplified lumped parameter model. A parametric study was carried out to understand the effect of stiffness and inertia of the rear structure on the façade performance. Shi et al. (2015) studied the effect of two forms of damage i.e., the pre-stress loss and anchorage failure on the dynamic behaviour of a cable net façade by finite element simulations. Various scenarios of single cable and multiple cables damages were analysed. The present paper demonstrates how the design of such cable-supported façades can be enhanced through the addition of a shape memory alloy (SMA) at one or both cable ends. One of the benefits of using SMA over other passive devices is its ability to absorb energy and also to recover large strains. Hence, the damage to the façade system is limited.

Shape memory alloy (SMA) is one type of smart material having several unique properties which can be used for various novel applications in structures. Foremost is the property of 'Shape Memory Effect' (SME) by which the material is able to memorise a shape. When it is heated beyond a certain transformation temperature, it attains its memorised shape if it is not restrained. If the SMA is fully or partially restrained during this process, then it develops recovery stress (or force). The other useful property of SMAs is that of 'super-elasticity' i.e., the ability to undergo large recoverable strains (typically up to 4-8%). Recovery stress and super-elasticity in SMAs have been the basis for its important applications in civil structures as outlined in several review papers (Janke et al., 2005; Cladera et al., 2014; Alaneme et al., 2019). Figure 1 shows a stress-strain curve depicting the super-elastic behaviour. The hysteresis loop formed during loading and unloading dissipates energy and reflects the damping capabilities of the SMA. SMAs have two stable phases – the high temperature austenitic phase and the low temperature martensitic phase. It is the diffusionless transformation from one phase to the other, achieved by applying either temperature (heating or cooling) or stress loading, that gives the SMA its unique properties. The most common variant of shape memory alloys is NITINOL (Nickel Titanium alloy), which has been widely applied in many systems including civil

structures. The major limitation of NITINOL is its high cost. In the past two decades, iron (Fe)-based SMAs have been developed, which are more cost effective.

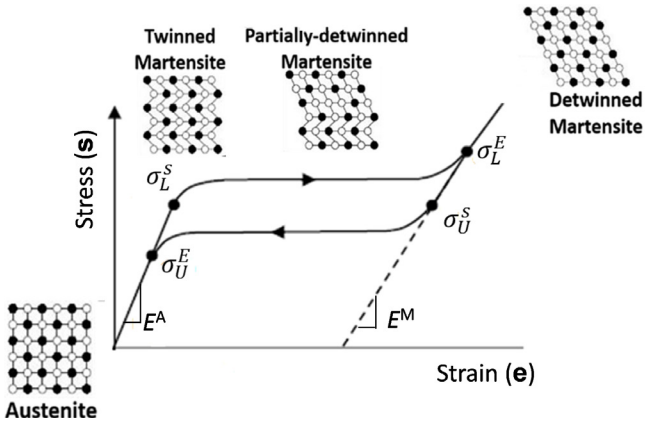


FIG. 1 Stress-strain behaviour of SMA implemented within ABAQUS user material model.

Janke et al. (2005) presented a comprehensive overview of SMA applications to civil engineering structures and cited some applications from 'Manside' (Brite Euram 1999) and 'Istech' (2000) projects. More recently Cladera et al. (2014) have provided an overview with emphasis on Fe based SMA applications. Cladera et al. (2014) have traced the development of Fe based SMAs over the past few decades, and have illustrated the use of the properties of SME, recovery stress, and damping towards improved designs of civil structures. Alaneme et al. (2019) have focused on applications of low-cost copper- and iron-based SMAs for vibration control of civil structures subjected to seismic loads. Gupta (2018a) presented a case study demonstrating the enhanced performance of a RC column wrapped by SMA wires under push over and seismic loading. Song et al. (2006) developed SMA-based passive, active, and semi-active control devices for civil structures. SMA-FRP-Steel hybrid reinforcements to beams, columns, and multi-storey buildings have been explored by Billah and Alam (2012), and Zafar and Andrawes (2015). The increased effectiveness of SMA cables as reinforcing elements in RC beams was shown by Mas et al. (2017). Andrawes and DesRoches (2007) and Wang et al. (2019) have explored use of SMA cable restrainers for the protection of bridges to earthquake excitation. Elfeki and Youssef (2017) examined optimum locations of SMA reinforcements in a building subjected to earthquake loading. Abraik and Youssef (2018) introduced super-elastic SMA rebars in plastic hinge locations on a steel reinforced concrete wall. Nahar et al. (2020) considered the beam and column joints for SMA reinforcements. Through analysis they have shown superior performance in terms of inter-storey and residual drift. Matthew et al. (2011) demonstrated the re-centring capability of a SMA-reinforced moment-resisting frame, which is desirable in sequential loading e.g., earthquake aftershocks.

While the applications of SMA in various civil structures have been the subject of investigation over the past several decades, its use in glazed façades has only recently attracted the attention of researchers. One of the motivating factors has been the developments in adaptive/smart façades as opposed to the traditional static façades, primarily to render them adaptable to external environmental inputs (Bedon et al., 2019). The second motivating factor has been to improve the structural resilience of traditional static façades when subjected to extreme wind and blast loads. There are primarily two approaches to SMA applications to structures. The first approach is actuator mode (active control) application using the property of shape memory effect (SME), requiring Joule

heating and mostly convective cooling. If strain recovery is constrained, large stresses or forces are induced which can alter the stiffness of the structure. The second approach, essentially a passive one, utilises the stress-induced super-elastic (SE) effect present in SMAs, and it does not require Joule heating. Both are powerful approaches, but different from each other in concept as well as in their practical applications. Dos Santos et al. (2014) using an active control approach with PID controller have proposed a 'bow string truss solution' for a smart glass façade, which can adapt its shape to wind loads. In another application (dos Santos et al., 2016a), SMA cables have been used in glass roof panels, in which external pre-stressing is induced by Joule heating utilising the property of the SME. More recently, dos Santos et al. (2020) have reported the development of an adaptive façade. Its shape (curvature) and position (in translation and in rotation) can be altered as per the requirement through antagonistic actuation of SMA wires utilising the property of SME and Joule heating. Gupta et al. (2019) reported use of a hybrid steel-SMA cable where SMA material cables were investigated at the ends of the steel cables. A case study was presented which showed improved structural integrity of the cable supported façade system resulting from the stress-induced super-elasticity (SE) benefits of the SMA.

In the present paper, the super-elasticity (SE) approach is further explored to gain an insight into the phenomenon and to study the effect of various parameters on the structural integrity of a hybrid SMA-Steel cable system. It is envisaged that this would result in less fragmentation and damage in the glazed system. The effects of various parameters, such as the proportional length and diameter of the SMA material (NITINOL) cable(s) are studied for a range of blast scenarios. The property of super-elasticity is considered within the context of blast-resilient glazing systems to help dissipate energy and allow damage recovery. SMA material is included by implementing a super-elasticity material model based on the stress-strain curves proposed in Qidwai and Lagoudas (2000). A detailed FE-model is developed in the commercial finite element software ABAQUS and the dynamic performance of the façade is studied. The potential benefits of including SMA within the cable connections to the main structure are explored. The paper is organised as follows: Section 1 introduces the problem undertaken in the paper and provides a review of available literature pertaining to various aspects of the same. Section 2 presents details of numerical modelling of a cable-supported façade to determine its dynamic response. This section also discusses the validation of the FE modelling of the prestressed cables using a lumped mass analytical model. Section 3 then considers a detailed parametric study to understand the behaviour of the façade with SMA cables at both ends. The effect of SMA cable length and its diameter, the primary design parameters of the steel-SMA hybrid cable, on the behaviour of façade is also examined. Finally, Section 4 presents conclusions from the present study.

## 2 NUMERICAL MODELLING

The general purpose finite element analysis (FEA) program ABAQUS is used for modelling and detailed analysis of the blast response of the façade systems. The dynamic analysis is performed and behaviour of the façade is investigated both with and without SMA. In the present application, the SMA used is Nickel-titanium alloy (NITINOL), which exhibits good super-elastic behaviour. Although iron-based shape memory alloys are more cost effective, the property of super-elasticity is practically absent in them and therefore they are not considered for the current application. The FE modelling of the cable-supported façade is briefly described below.

Cables or cable trusses utilise tension-only members to support glazing systems. In the present work, a hybrid SMA-Steel tensioned cable system is proposed, in which SMA wire is provided at the interface with the main support structure at both ends.

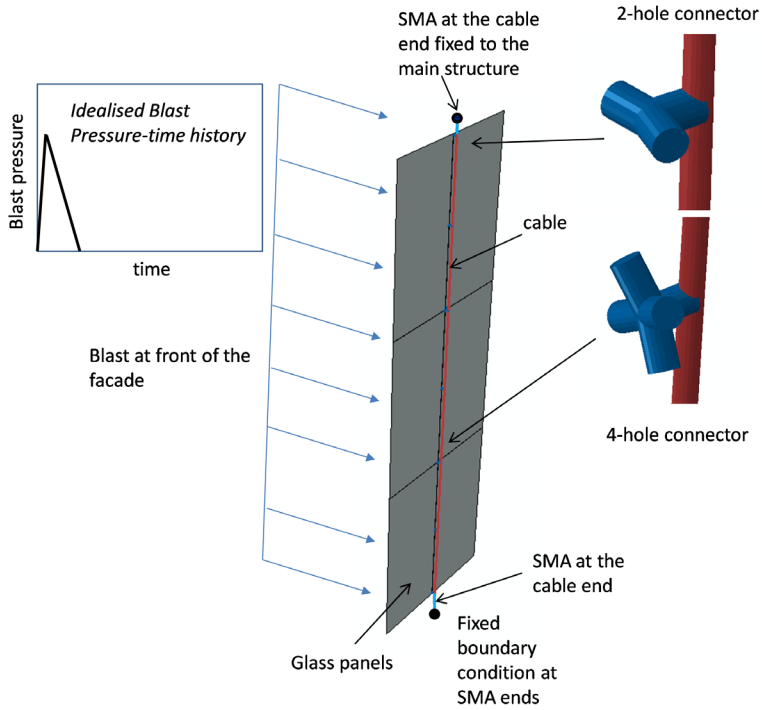


FIG. 2 FE model of the cable supported façade with SMA elements included at both ends

The façade considered measures 10m tall and consists of laminated glass of 1.5 m width and 3.2 m height (Figure 2). Lateral restraints were ignored, since the façade was assumed to be sufficiently wide. Therefore, only one bay of 1.5m width was considered for analysis. Each panel was assumed to be supported on six point supports. A four-hole spider connector was used in the corner for connecting four adjacent panels to the cable, while a two-hole connector was introduced at the middle of the vertical edges for additional point supports. The laminated glass comprises two 10mm layers of fully tempered glass bonded by a 1.52mm thick PVB interlayer. The high strength steel cables were of 32mm diameter. The cables were pre-tensioned to a load of 150kN. The SMA member attached to the steel cable was also a cable of 32mm diameter and a length of 250 mm. In the parametric study both the SMA cable length and diameter were varied over a range to understand their effect on façade dynamic response.

Cables were modelled using cable elements and were assigned elastic behaviour of steel (Young's modulus = 130GPa, Poisson's ratio = 0.3 and density = 7850kg/m$^3$). The glass panels were modelled using shell elements of 21.52mm thickness. The glass panels were modelled as a monolithic unit with elastic properties (Young's modulus 70GPa, Poisson's ratio = 0.2, density = 2500kg/m$^3$). This is considered suitable for analysing the façade prior to glass breakage. The objective of the study is to investigate the cables and their connections to the main structure, which are the critical components of the cable-supported façade system. The glass was included in the model to account for its mass participation in the dynamic response and for transferring the loads to the cables. Spider brackets

were modelled using rigid beam elements and constraints were applied to connect them with the glass and cable. For the finite element analysis, the cable was discretized using a mesh size of 0.01m for the truss element, while glass panels were discretized using 0.05m for shell element. A mesh sensitivity analysis was conducted to ensure that the chosen mesh size was reasonable for the purpose of the present study. Boundary conditions were imposed on the model. These included the pinned but fixed-in-position boundary condition at the ends of the cable where it connects to the structure and symmetry boundary conditions at the ends of the modelled width of the bay.

TABLE 1 Material properties of SMA used in ABAQUS user material model (Qidwai & Lagoudas, 2000)

| PROPERTY | SYMBOL | UMAT PARAMETERS |
|---|---|---|
| Austenite elasticity (GPa) | $E_A$ | 70 |
| Austenite Poisson's ratio | $\nu_A$ | 0.33 |
| Martensite elasticity (GPa) | $E_M$ | 30 |
| Martensite Poisson's ratio | $\nu_M$ | 0.33 |
| Transformation strain | $\varepsilon^A$ | 0.05 |
| Start of transformation loading (MPa) | $\sigma^s_L$ | 440 |
| End of transformation loading (MPa) | $\sigma^E_L$ | 540 |
| Reference temperature (degC) | $T_0$ | 22 |
| Start of transformation unloading (MPa) | $\sigma^s_U$ | 250 |
| End of transformation unloading (MPa) | $\sigma^E_U$ | 140 |

The material model was implemented within ABAQUS which captured the super-elastic behaviour of SMA. The user material model (UMAT) parameters used in the present analysis are given in Table 1. The Young's modulus for the austenite phase $(E_A)$ is 70GPa and for the martensite phase $(E_M)$ is 30GPa. The stress-strain behaviour illustrated in Figure 1 is at a temperature higher than the austenitic finish temperature $A_f$, and phase transformations during loading and unloading of SMA are primarily stress induced. During loading of SMA, austenite to martensite transformation starts at a stress level of $\sigma_L^S$ and is complete at stress $\sigma_L^E$. During unloading the reverse transformation i.e., martensite to austenite begins at stress level of $\sigma_U^S$ and ends at stress $\sigma_U^E$.

The analysis was conducted in ABAQUS using the dynamic implicit solver. The FE model of the façade developed is shown in Figure 2. The dynamic analysis is used to generate the response of the façade taking account of dynamic interaction between the blast load, glazing, and the cables. In order to have sufficient confidence in the trends of results generated by detailed façade FE analysis described above, an alternative simplified lumped parameter model similar to the one proposed by Royer-Carfagni and Vivian (2020) was developed and utilised.

## 2.1 LUMPED PARAMETER MODEL AND COMPARISON WITH FEA RESULTS

A hypothetical three degree-of-freedom (3DOF) model of a cable façade shown in Figure 3 is considered here. It is a simplified model without SMA where the total cable length is subdivided in four parts. The top and bottom ends of the pre-tensioned cable are pinned but fixed in position. The mass of the glass panels and the cables is lumped at three points along the cable. The lumped masses on the cable align with the centre of each glass panel. It can be assumed that each mass

representing a glass panel is attached to the cable through a single point fictitious connection at the centre of the panel. The model is symmetrical with respect to the cable midpoint. Numerical values of the cable and lumped mass parameters of the 3DOF model compared well with the detailed FE modelling described above. The difference between the two models lies in the details of connection between the glass panels to the cable. In the façade FE model the connections are as per actual configuration as shown in Figure 2 i.e., four-hole spider connection at the corner and two-hole connector at the mid-point of the glass panel edge, whereas in the 3DOF model it is a fictitious single point connection at the glass panel centre. A transient force representing blast loading on the glass panel is applied on each of the three masses.

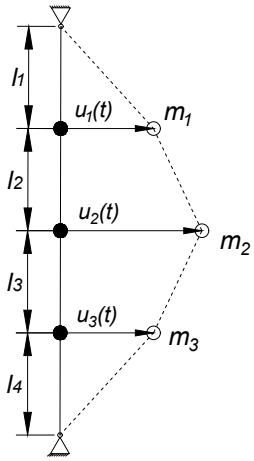

FIG. 3 3DOF lumped mass model

In the deformed configuration, both the cable pre-tension $(T_0)$ and its extensional stiffness $(E_i A_i / L_i)$ contribute to total strain energy, which is given by,

$$U = T_o L + \frac{1}{2}\sum_{i=1}^{4} \frac{E_i A_i}{L_i} L_i^2 \tag{1}$$

Here $L$ is the total change in cable length given by $\sum_i L_i (i = 1 \ldots 4)$. $L_i$ is the change in the length of the $i^{th}$ cable segment given by,

$$L_i = \sqrt{L_i^2 + (u_i - u_{i-1})^2} - L_i \tag{2}$$

Here $u_0$ and $u_4$ are equal to zero being the displacements in transverse direction at the cable ends. The system kinetic energy in terms of three lumped masses is given by,

$$V = \frac{1}{2}\sum_{i=1}^{3} m_i \dot{u}_i^2 \tag{3}$$

Lagrangian is given by $L = V - U$ . Application of Lagrange's equation and setting the right-hand side equal to external forces $F_i$ leads to three coupled non-linear equations of motion. These equations were solved by numerical integration to calculate the cable response.

The data for the 3DOF lumped parameter model is derived from the detailed FE model. The four lengths $l_1, l_2, l_3$ and $l_4$ are assumed to be 1.83m, 3.22m, 3.22m, and 1.83m, respectively. The lumped masses $m_1, m_2$ and $m_3$ at three points on the cable are 258kg, 262kg, and 258kg, respectively, which correspond to a mass of 1.5m x 3m x 21.52mm thick glass panel and half the length of the cable on either side of the lumped node. The pretension as well as material properties of the cable are assumed to be the same as those described in previous section for the detailed FE model.

The lumped parameter system was also modelled in ABAQUS following the FE modelling approach similar to that for the main façade system described in the previous section to ensure the solution was representative and a good comparison was observed. The model comprises the single cable of same size and length as in the detailed FE model and lumped masses which represent the glass panels. For the initial assessment and validation, a blast scenario of a 100kg TNT charge at 40m standoff is considered. This would result in an approximate peak blast pressure of 40kPa and duration 20ms based on Kingery-Bulmash empirical equations (1984). An idealised pressure-time profile in the form of a triangular pulse (Figure 2) comprising only a positive phase was assumed for the purpose of the study. The triangular pulse was assumed to have an almost instantaneous rise to the peak pressure of 40kPa and then linear decay for a duration of 20ms. The corresponding impulse is 400kPa-ms. In the detailed FE model, blast pressure was applied uniformly on the entire façade, whereas in the lumped mass model, a concentrated load at the three nodes was calculated using the tributary area of the glass panel.

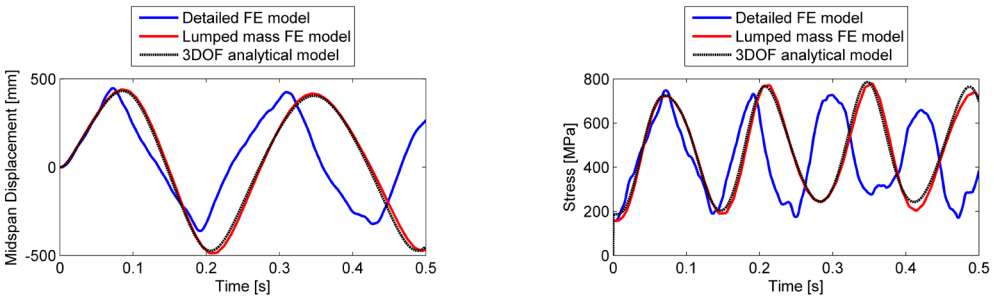


a b

FIG. 4 Comparison of cable midspan (a) displacement and (b) stress for 40kPa-20ms blast load from Detailed façade FE model, Lumped mass FE model, and 3DOF system analytical model

For the considered blast load, a preliminary comparison of cable midspan displacement and stress response from three analyses is presented in Figure 4a and Figure 4b. These three analyses are: solution of the detailed façade FE model (Figure 2) and the 3DOF lumped parameter model (Figure 3) solved by two different methods i.e., direct numerical integration of equations of motion and FE analysis in ABAQUS. Cable displacement and stress responses of the 3DOF model by FE analysis and from direct numerical integration solution agree very well with each other, as shown in Figure 4a and Figure 4b. This indicates that the analytical solution is able to capture the fundamental behaviour of the system. Note that the basic features of FE modelling in ABAQUS are same for the 3DOF system and for the main façade system. Cable displacement and stress responses from the solution of

the detailed FE model of the façade system are also superimposed in Figures 4a and 4b. These responses are reasonably well matched, from a qualitative perspective, with that of the 3DOF system. The quantitative difference in the results can be attributed to the differences in the modelling of the glass panel and its connection to the cable. Note that in the façade FE model, the cable is discretized using cable elements, whereas the glass panels are discretized using shell elements. Therefore, it is an elaborate FE model, as it has a large number of elements and degrees of freedom. In the lumped mass FE model, the discretization of the cable-utilizing truss element is similar to that in the façade FE model, however the glass panels are represented by point masses assumed to be connected to the cable at the panel central point. The façade FE model predicts similar inward (the first peak in Figure 4a) cable midspan displacement, though peak to peak displacement is slightly lower compared to the lumped mass FE model. In Figure 4b, the peak stress values of the two approaches match reasonably well. The natural frequency predicted from the façade detailed FE model is slightly higher than that obtained from the lumped mass FE model, possibly due to the additional strain energy stored in the glass panels. The overall correlation of results in Figures 4a and 4b provides sufficient confidence in FE models of both the façade and of the 3DOF system. The parametric study presented in Section 3 is performed using the detailed façade FE model.

# 3 ANALYSIS OF FAÇADE SYSTEM AND PARAMETRIC STUDY

For initial assessment, the same blast scenario of 40kPa peak pressure and 20ms duration as in the previous section was considered. It was assumed that the entire façade would be uniformly loaded by the blast pressure and therefore did not account for the effect of phasing. For a real design, this is a conservative assumption as the façade at a higher level will usually experience less loading in comparison to the façade at ground level. However, since the purpose of the study is to investigate the effect of including SMA in the façade, a more complex blast loading scenario is not deemed necessary.

## 3.1 INITIAL ASSESSMENT RESULTS

The results for the blast load of 40kPa peak pressure and 20ms duration are presented in this section. The analyses have been conducted for three configurations of the façade (a) without SMA, (b) with SMA at one end, and (c) with SMA at both ends. The length of SMA cable at one end as well as at both ends is 250mm while the diameter is 32mm, which is same as that of the steel cable. The results for the three cases are summarised in Table 2.

TABLE 2 Maximum façade response for blast load of 40kPa peak pressure and 20ms duration

| | WITHOUT SMA | WITH SMA AT ONE END | WITH SMA AT BOTH ENDS |
|---|---|---|---|
| Support Reactions (kN) | 864 | 617 | 400 |
| Deflections (mm) | 450 | 486 | 508 |
| Maximum stress in the Cable (MPa) | 1082 | 830 | 530 |

The deformed shape of the façade, when subjected to the blast load, for the case when the SMA cable is not used, is shown in Figure 5a. A similar deflected shape where the cable displacement is maximum around the midspan and is minimum at both the ends is observed when the SMA is

used. The mid-span displacement time-history of the cable for the three cases i.e., without SMA, with SMA at one and both ends, is shown in Figure 5b. The midspan cable response is cyclic, and it is observed that the peak displacement of the façade increased slightly due to the inclusion of SMA. The maximum displacement occurs in the first cycle, which corresponds with the inward motion of the cable. The maximum displacement of the façade without SMA and with SMA at both ends is 450mm and 508mm, respectively. This larger displacement is attributed to the larger strains predicted in the SMA material which help soften the response.

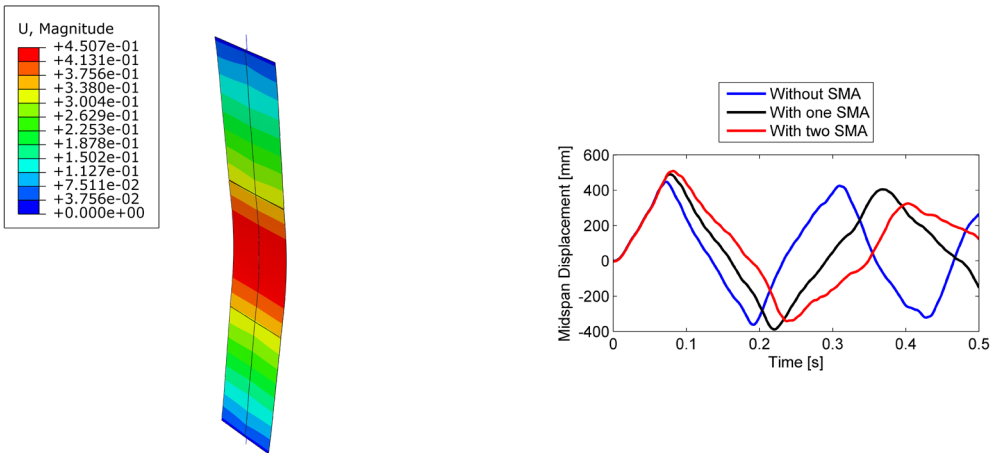


a b

FIG. 5 (a) Maximum inward deformation (meters) of the façade without SMA and (b) mid-span displacement time-history of the cable for the façade system without and with SMA at one and two ends

The resultant of the reaction forces at the end of the cable and the maximum axial stress experienced by the cable are shown in Figures 6a and 6c. It can be observed that with inclusion of SMA, the reaction force and stress in the cable are considerably reduced, the reduction being substantially more for the case when SMA cable is used at both ends. Comparing the case without SMA with the case that has SMA at one end, reduction in the peak stresses from 1082MPa to 830MPa and peak support reactions from 864kN to 617kN are observed. For the case with SMA at both ends, support reactions and cable stresses are reduced to 400kN and 530MPa, respectively.

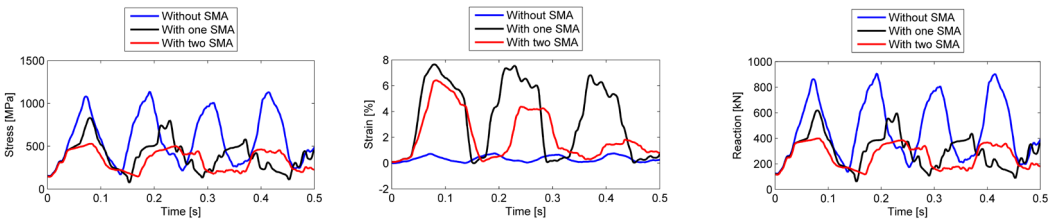


a b c

FIG. 6 Maximum (a) stress, (b) strain, and (c) reaction force at the cable end for 40kPa-20ms blast load for the façade system without SMA and with SMA at one and two ends

The behaviour of SMA for the two cases i.e., SMA at one end and SMA at both ends can be understood from the strain time history in Figure 6b and the stress-strain plot for SMA given in Figure 7a. In the case of SMA at one end, the strain is very high, exceeding 7%, whereas for the case of SMA at both ends the maximum strain is within about 6.2%. The significance is that SMA cable at one end is approaching its limit with little margin for overloading, whereas SMA cables at both ends have some strain margin to accommodate additional load. When SMA strain exceeds about 7% as in the case of one SMA, there is complete transformation from austenitic to high stress detwinned martensitic phase (Figure 1). For the case of two SMAs, where the maximum strain is less than about 6.2%, incomplete transformation from austenite to partially-detwinned martensite takes place.

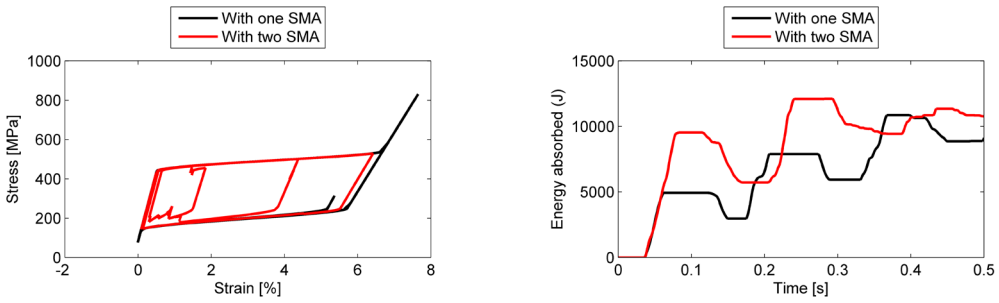


a b

FIG. 7 (a) Behaviour of SMA at (40kPa-20ms) blast loading and (b) strain energy absorption within SMA for the façade enhanced with SMA at one end of the cable and SMA at both ends

Large deformation/strain of the SMA due to its property of super-elasticity results in effectively absorbing more energy, which is the primary reason for reduced cable reactions and stresses. This is apparent in the response of the façade system with SMA at one end as well as SMA at both ends (Figures 6a and 6c), which demonstrate the benefits of including SMA in the design. Figure 7b gives the energy absorption for the two cases of one SMA and two SMA. The overall energy absorption for the case of two SMA is greater than in the case of one SMA. For the case where one SMA was included, the SMA was overstrained (maximum stress of about 830 MPa) in comparison to the scenario where SMA at both ends was included, with peak stress of around 530 MPa. It should be noted that maximum cable stress is observed near the support, so when SMA is included at the end of the cable, the stress is at its maximum in the SMA section of the hybrid cable. To ensure an acceptable or superior performance of the façade, the selected SMA elements should have an adequate ultimate strength. For the extreme load scenario, it is recommended that SMA is included at both ends of the cable as this will allow limiting strains in the SMA and extract maximum benefit. It is worth mentioning that the steel cables were modelled as elastic and no failure criterion was imposed. The ultimate tensile strength of Ni-Ti alloy is typically in the range of 800-1500 MPa in austenitic phase and 700-2000MPa in martensitic phase (Janke et al., 2005). Similarly, a typical strength of the spiral strand type cable made of stainless steel is about 1570MPa (Piyasena et al., 2019). For the case in which SMA is included at both ends, the stresses in the cable are well below the strength, and therefore failure of the façade system would be prevented. For the considered extreme loading scenario, it is demonstrated that the façade with SMA cables at both ends would be more resilient in terms of reduced cable stresses and support reactions.

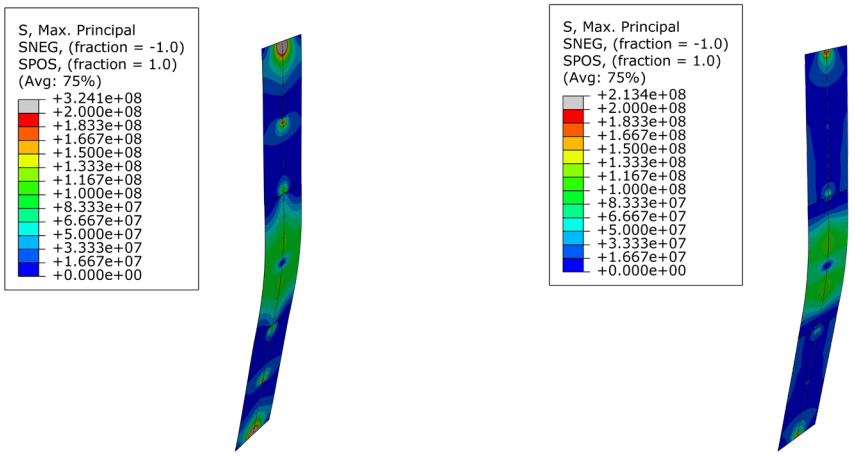


*a* *b*

FIG. 8 Maximum principal stress (Pa) in glass panels at the time of maximum façade displacement due to blast load of 40kPa-20ms for the case (a) without SMA and (b) with SMA at both ends

Glass stresses were also studied to assess the effect of introducing SMA at both ends. Stress plots for the blast load under consideration i.e., 40kPa peak pressure and 20ms duration are shown in Figures 8a and 8b for the cases without SMA and with SMA at both ends. The nature of stress distribution as well as magnitude is generally comparable in both cases. The stresses within the panels are generally uniform, with some small, localized regions of high stress at the points of connection of the panels to the cable. It is noted that stresses in the glass are at their maximum near the cable ends where the structure is most stiff. The maximum stress in the glass as shown in Figure 8a is predicted to be about 324 MPa in a localised region near the cable ends. This stress level, however, is hypothetical, since the glass would crack well below this stress value. The peak stress reduced to around 213MPa when SMA was introduced at both ends. In the present analysis, breakage of the glass was not modelled, but it is expected that the glass panels near to the cable ends would break as the glass stresses locally near the supports were in excess of 200MPa which is a typical value of dynamic strength of a tempered or toughened glass (Cormie et al., 2009). It is envisaged that the worst consequence would be the failure of cables and therefore the focus in the present study is on studying the behaviour of the cables. The influence of breakage of the glass on the overall façade response is not studied in detail. It is expected that breakage of glass will reduce the demands on the cable due to dissipation of some blast energy in the cracking of the glass, but is not expected to alter the cable response significantly. It is therefore deemed reasonable to ignore glass breakage in present study which focusses on plausible failure of cables and their connections due to high stresses and support reactions.

In the above assessment, it is shown that the failure of cables which can result in catastrophic failure can be prevented by including SMA at cable ends. For the loading scenario considered, a significant improvement is observed in the performance of the façade in terms of reduction in the cable stresses and support reactions when SMA was introduced in the design.

## 3.2 PARAMETRIC STUDY

To better understand the behaviour of the cable-supported façade with SMA, a parametric study is conducted using the full façade model described in section 2. The intensity of the blast load, the length of the SMA included at the ends of the cables, and the diameter of the SMA cable relative

to the diameter of the steel cable are three parameters considered here and their influence on the dynamic performance of the façade is studied.

### 3.2.1 Influence of Loading

A load of 100kg TNT charge at 40m standoff, which corresponds to a blast load of 40kPa and a duration of 20ms was initially considered in sections 2 and 3.1. Subsequently, two more blast loads are considered, one of lower intensity i.e., 25kPa peak pressure and duration of 14ms corresponding to 40kg TNT at 40m standoff, and a higher intensity blast of 87kPa peak pressure and 12.5ms duration corresponding to 100kg TNT charge at 25m standoff. Assuming a triangular pulse, these three load levels correspond to an impulse of 175kPa-ms, 400kPa-ms, and 544kPa-ms. These blast scenarios are designated as loads 1, 2, and 3, respectively and are summarised in Table 3. In this section, only the case of SMA at both ends is considered.

TABLE 3 Summary of considered blast load cases

| BLAST LOAD CASE | PRESSURE (kPa) | DURATION (ms) | IMPULSE (kPa-ms) |
|---|---|---|---|
| **Load 1** | 25 | 14 | 175 |
| **Load 2** | 40 | 20 | 400 |
| **Load 3** | 87 | 12.5 | 544 |

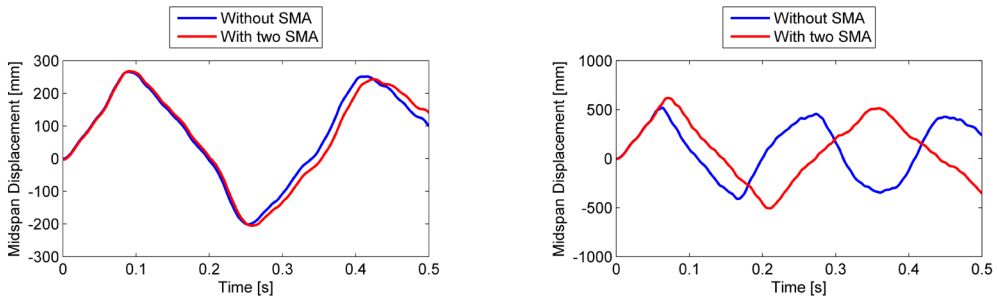


a b

FIG. 9 Mid-span displacement of cable for (a) load 1 (25kP-14ms) and (b) load 3 (87kPa-12.5ms)

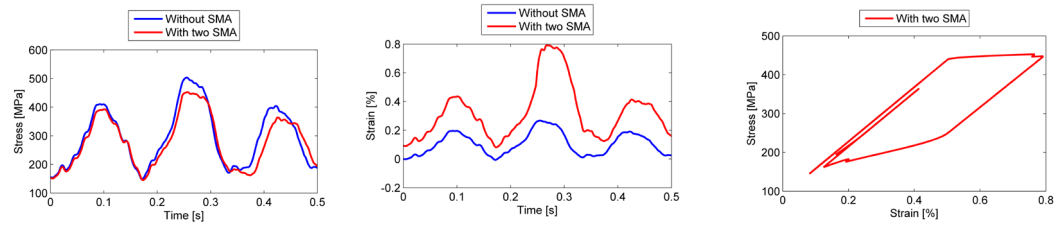


a b c

FIG. 10 (a) Peak cable stress, (b) strain response, and (c) the stress-strain behaviour of SMA for load 1 (25kPa-14ms)

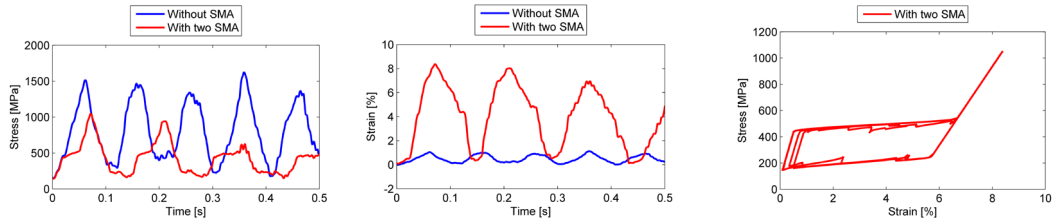


a b c

FIG. 11 (a) Peak cable stress, (b) strain response, and (c) the stress-strain behaviour of SMA for load 3 (87kPa-12.5ms)

Figures 9a and 9b give the cable midspan displacement for the cases without and with SMA for loads 1 and 3, respectively. The difference in cable displacements for two cases of without and with SMA is marginal in load 1 and is more pronounced in the case of load 3. There is a decrease in the natural frequency of the system with use of SMA cable ends, which is marginal in the case of load 1 but is more pronounced in the case of load 3. Figures10a and 10b show the peak cable stress and strain response and the corresponding stress-strain behaviour of SMA for the case of load 1 is given in Figure 10c. The reduction in stresses with SMA cable ends is marginal. The corresponding strain developed in the cable is also small i.e., the maximum strain is less than 1%.

For load 3, the reduction in cable stress with SMA included is significant (Figure 11a), accompanied by a relatively larger strain of about 8% (Figures 11b and 11c). For load 3, SMA cables are strained to their limit (~8% as shown in Figures 11b and 11c), whereas for load case 2, the SMA cables are strained up to about 6.2% (Figures 6b and 7a). The peak cable stresses, midspan displacement, and support reactions for the three load cases and the percentage reduction in their magnitude with the use of SMA at cable ends are summarised in Table 4. It is evident that the beneficial effect of using SMA is more pronounced for higher blast loads where glass breakage is more likely. Maximum advantage is achieved when the behaviour of SMA is limited to transformation phase where it remains in the state of partially-detwinned martensite. This behaviour is observed in load case 2 with two SMA as shown in Figure 7a. In load case 3 of higher blast load, SMA completely transforms into detwinned martensite (Figure 11c) and this results in relatively higher stress (Figure 1) in the cable, which may lead to failure despite using SMA.

TABLE 4 Maximum façade response for load cases 1 (25kPa-14ms), 2 (40kPa-20ms), and 3 (87kPa-12.5ms)

| | WITHOUT SMA | WITH SMA AT BOTH ENDS | % CHANGE |
|---|---|---|---|
| **Support Reactions(kN)** | | | |
| Load 1 | 330 | 313 | -5.15% |
| Load 2 | 864 | 400 | -53.70% |
| Load 3 | 1206 | 772 | -35.98% |
| **Deflections (mm)** | | | |
| Load 1 | 267 | 267 | 0% |
| Load 2 | 450 | 508 | 12.89% |
| Load 3 | 536 | 617 | 15.11% |
| **Cable/SMA stresses (MPa)** | | | |
| Load 1 | 411 | 391 | -4.86% |
| Load 2 | 1082 | 530 | -51.02% |
| Load 3 | 1516 | 1045 | -31.07% |

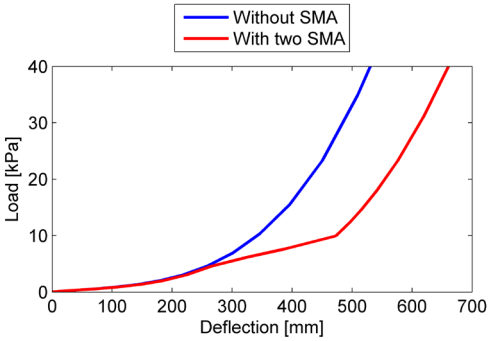


FIG. 12 Resistance function of the façade based on static pushover analysis

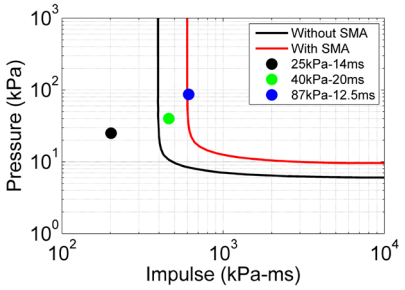


FIG. 13 Pressure-impulse curve for cable supported façade with and without SMA for the damage level corresponding to the cable stress of 1000MPa

To further illustrate the margins of safety for the façade system with SMA, pressure-impulse (PI) curves have been generated using single degree of freedom (SDOF) representation of the system. The mass of the equivalent SDOF takes account of the mass of the cables and glass panels participating in the response.

The resistance of the façade system is calculated by conducting a pushover analysis, where the façade is laterally loaded by applying a gradually increasing static pressure. The resistance function in terms of the applied pressure and the deformation of the façade is shown in Figure 12. It can be seen that initially at relatively small loading, both façades without and with SMA respond in a similar manner. As the load increases, the response of the façade with SMA deviates. With SMA, the response is observed to be more flexible, thereby permitting larger deflections. At large deflections, the resistance increases sharply due to membrane action of the cables. An equivalent SDOF system based on the nonlinear resistance function and the mass corresponding to the mass of the cables and glass panels participating in the dynamic response is iteratively solved to develop the iso-damage or pressure-impulse (PI) curves. These PI curves exhibit the performance of the façade over the entire range of loading from very impulsive to quasi-static regime. The PI curves are plotted for a given level of damage and different loading scenarios characterised by the load-impulse combination. In the present study, these are developed for a damage state corresponding to the cable stress of 1000MPa. The PI curves for the façade without and with SMA are shown in Figure 13. Superimposed on the same graphs are the pressure-impulse points corresponding to the three blast scenarios considered. It can be seen that the point corresponding to the highest blast load 3 (544kPa-ms impulse due to 87kPa peak pressure with 12.5ms duration) lies just above and to the right of the PI curves for both façades i.e., with and without SMA. This indicates that the cable stresses have exceeded the limit of 1000MPa. The pressure-impulse point for the lowest blast load (175kPa impulse due to 25kPa peak pressure with 14ms duration) lies below and to the left of both PI curves, which indicates that the stress level in the cable remains well below 1000MPa for both façades. The point for the blast load case 2 (400kPa-ms impulse due to 40kPa peak pressure with 20ms duration) indicates that in the façade with SMA the cable stresses are below 1000MPa, whereas for the façade without SMA the cable stresses have exceeded 1000MPa. From Figure 12, it can also be observed that for static loads of up to 7kPa, the behaviour of the façade with and without SMA is comparable. Hence, the use of SMA doesn't compromise the performance of the façade for conventional wind loads, but enhances the performance of the façade for extreme loads of impulsive and dynamic nature.

The results clearly demonstrate the benefits of using SMA at both ends in the cable-supported façade for extreme load conditions.

### 3.2.2 Influence of SMA Cable Length

A sensitivity study to investigate the influence of the length of the SMA element was also considered. The analysis was performed for the midrange blast load 2 of 40kPa peak pressure for 20ms duration. Four different lengths of SMA at both cable ends were taken. These were 100mm, 250mm, 500mm, and 1000mm at each end. The results of this assessment are summarised in Table 5.

TABLE 5 Influence of length of SMA cable at each end for blast load of 40kPa-20ms.

| SMA LENGTH AT CABLE ENDS | FACADE WITHOUT SMA | 100mm SMA CABLE | 250mm SMA CABLE | 500mm SMA CABLE | 1000mm SMA CABLE |
|---|---|---|---|---|---|
| Support reactions (kN) | 864 | 668 | 400 | 395 | 395 |
| Façade deflection (mm) | 450 | 481 | 508 | 510 | 513 |
| Cable/SMA stresses (MPa) | 1082 | 899 | 530 | 520 | 520 |
| SMA strain (%) | - | 7.9 | 6.41 | 5.9 | 5.8 |

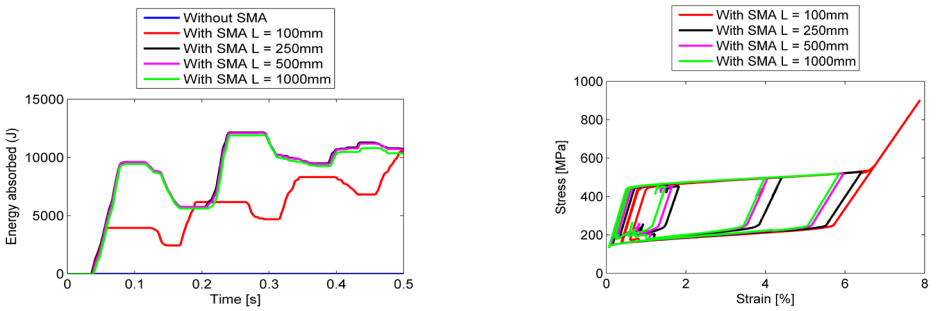


a b

FIG. 14 (a) Whole façade model strain energy absorption and (b) stress-strain behaviour of SMA for different lengths of SMA at both cable ends

It can be seen that by increasing the SMA length, the performance of the façade improves in terms of reduced cable stresses and support reactions. For the present configuration, it is noted that the increase in the SMA length up to 250mm at each end provides sufficient benefit. No further significant improvement is achieved beyond the cable length of 250mm. The strain energy absorption of the whole model for the four cases of different SMA lengths is shown in Figure 14a. It can be seen that the system with SMA length of 250mm allows for significant higher energy absorption in comparison to the case in which only 100mm long SMA element was considered at both ends. For the case of SMA lengths of more than 250mm, the energy absorption is comparable and only a slight variation is observed due to different parts of the SMA section becoming stressed to different levels. To better understand that, the stress-strain behaviour of SMA of different lengths is examined in Figure 14b. It can be observed that for the case of SMA of length $L$ = 100mm, the strains are high and the SMA is completely transformed to de-twinned martensite, whereas for all other lengths, the SMA is not completely transformed and remains in the partially de-twinned martensite state. Hence, the optimum design for a particular loading would be to choose

a minimum length of SMA so that its behaviour is limited to partial transformation into de-twinned martensite phase, Figure 1.

### 3.2.3 Influence of SMA Cable Diameter

Finally, a sensitivity study to investigate the influence of SMA cable diameter was also considered. The analysis was performed for the midrange blast load of 40kPa peak pressure for 20ms duration. Three different diameters of SMA of 25mm, 32mm, and 36mm were investigated, keeping the SMA length fixed to 250mm. The results of this assessment are summarised in Table 6. The comparison of the peak stress and reactions for all cases is given in Figures 15a and 15b, respectively. In general, the reduction in the support reaction and stresses is observed when SMA is included. The support reactions are reduced by practically a similar amount for all cases of SMA diameters. As shown in Table 6, these are in the range of 400kN to 491kN, typically a reduction of about 50%. However, the peak stress is only reduced appreciably for the case of higher diameters (i.e., for $d = 32$mm and 36mm) i.e., in the range of 506MPa to 530MPa compared to the value of 1082MPa when SMA is not used. Figure 15c shows the stress-strain behaviour of SMA for different diameters. For the case of SMA with a smaller diameter of 25mm, a full transformation of SMA to detwinned martensite is observed, hence the stresses are relatively higher, whereas for the case of SMA with larger diameters (32mm and 36mm), the stresses are capped due to SMA behaviour restricted to partial transformation phase.

TABLE 6 Influence of diameter of SMA cable at each end for blast load of 40kPa-20ms

| SMA CABLE DIAMETERS | FACADE WITHOUT SMA | 25mm SMA CABLE DIA | 32mm SMA CABLE DIA | 36mm SMA CABLE DIA |
|---|---|---|---|---|
| Support Reactions (kN) | 864 | 450 | 400 | 491 |
| Façade deflection (mm) | 450 | 550 | 508 | 475 |
| Cable/SMA stresses (MPa) | 1082 | 995 | 530 | 506 |
| SMA strain (%) | - | 8.2 | 6.41 | 4.6 |

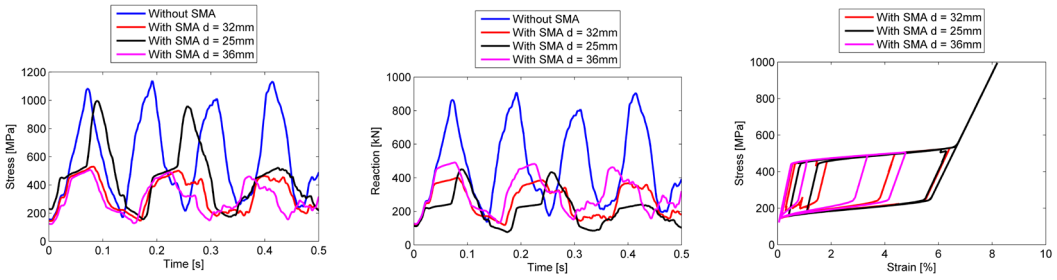


a b c

FIG. 15 (a) Peak stress, (b) reaction, and (c) stress-strain behaviour of SMA for different diameters of SMA cable at both ends for a blast load of 40kPa-20ms

Therefore, to maximise the benefit of SMA for a particular design loading scenario, the SMA diameter and length should be chosen to limit its behaviour to the transformation phase where it remains in a partially detwinned martensite state. The region of complete transformation to detwinned martensite beyond the stress level of $\sigma_L^E$, which also has a steep rise in stress, is to be avoided in order to limit

the support reactions and cable stresses. It will also prevent sudden changes in the façade stiffness that could result in high dynamic reactions. An optimal design situation will be one in which the SMA is strained to a sufficiently high strain, yet remains in the partially detwinned martensitic phase e.g., the 250 mm length case in Figure 14b. It would also be desirable to have some margin to avoid the fully detwinned martensite region, due to an unexpected increase in the design blast load.

## 4 CONCLUSIONS

In this paper, the application of super-elastic NITINOL in improving the blast resilience of cable-supported façades has been explored and results from ongoing research are discussed.

SMA, due to its property of super-elasticity, has an enhanced ability to absorb and dissipate energy, which is shown to be beneficial towards improving the structural integrity of the façade. Results indicate that by providing short lengths of SMA cables at one or both ends of the cable façade system, considerable reduction in the cable stresses and support reactions can be achieved. This is, however, at the expense of slightly higher deformations. Reduction in peak glass stresses, which are at a maximum near the cable ends, is also observed. This would be an added advantage of using SMA in the façade that could support the use of thinner glass which would be an appealing saving.

At higher (extreme) loads it is found that the beneficial effect of using SMA is more pronounced, and SMA at both cable ends is more effective compared to SMA at one end. Analysis also shows that there exists an optimum length of SMA cable at both ends, which practically provides the greatest reduction in cable stresses and support reaction. Increasing the SMA cable length beyond this value gives only a marginal improvement. A sensitivity study performed on the SMA cable diameter indicates that support reactions are reduced for all selected diameters. However, to achieve a reduction in stresses, a diameter of SMA cable which limits its behaviour to a partial detwinned phase should be chosen. In order to make best use of the SMA properties, it should be employed at both top and bottom of the support system and cable parameters should be chosen so that the SMA develops a reasonably high strain, yet remains in the partially detwinned martensitic phase.

Pushover analysis of the façade reveals that the introduction of SMA at both cable ends does not compromise the performance of the façade for conventional wind loads, but enhances the performance of the façade for extreme loads of impulsive and dynamic nature. The pressure impulse (PI) curves also clearly show that for a particular blast load, the introduction of SMA would reduce the risk of failure of the façade.

It is concluded that the blast performance of a cable-supported façade system can be improved through the inclusion of SMA components.

### References


Abraik, E. & Youssef, M. A. (2018). Seismic fragility assessment of superelastic shape memory alloy reinforced concrete shear walls. *Journal of Building Engineering*, *19*, 142-153.

Alaneme, K. K., Okotete, E. A., & Anaele, J. U. (2019). Structural vibration mitigation – a concise review of the capabilities and applications of Cu and Fe based shape memory alloys in civil structures. *Journal of Building Engineering*, *22*, 22-32.

Amadio, C. & Bedon, C. (2012a). Elastoplastic dissipative devices for the mitigation of blast resisting cable-supported glazing façades. *Engineering Structures*, *39*, 103-115.

Amadio, C. & Bedon, C. (2012b). Viscoelastic spider connectors for the mitigation of cable-supported façades subjected to air blast loading, *Engineering Structures*, *42*, 190–200.

Andrawes, B. & DesRoches, R. (2007). Comparison between shape memory alloy seismic restrainers and other bridge retrofit devices. *Journal of Bridge Engineering*, *12*(6), 700-709.

Bedon, C. & Amadio, C. (2014). Exploratory numerical analysis of two-way straight cable-net façades subjected to air blast loads. *Engineering Structures*, *79*, 276–289.

Bedon, C., Honfi, D., Machalická, K. V., Eliášová, M., Vokáč, M., Kozłowski, M., Wüest, T., Santos, F., & Portal, N. W. (2019). Structural characterisation of adaptive façades in Europe – Part I: Insight on classification rules, performance metrics and design methods. *Journal of Building Engineering*, *25*, 100721.

Bedon, C., Zhang, X., Santos, F., Honhi, D., Kozlowski, M., Arrigoni, M., Figuli, L., & Lange, D. (2018). Performance of structural glass façades under extreme loads- Design methods, existing research, current issues and trends. *Construction and Building Materials*, *163*, 921-937.

Billah, A.H.M.M. & Alam, M.S. (2012). Seismic performance of concrete columns reinforced with hybrid shape memory alloy and fiber reinforced polymer bars. *Construction and Building Materials*, *28*, 730-742.

Brite Euram. (1999). MANSIDE project - memory alloys for new seismic Isolation and energy dissipation devices. *Proceedings of the final project workshops*, Rome, Italy.

Cladera, A., Weber, B., Leinenbach, C., Czaderski, C., Shahverdi, M., & Motavalli, M. (2014). Iron-based shape memory alloys for civil engineering structures: An overview. *Construction and Building Materials*, *63*, 281-293.

Cormie, D., Mays, G., & Smith, P. (2009). *Blast effects on buildings ( 2nd ed.)*. Thomas Telford.

dos Santos, F. A., Bedon, C., & Micheletti, A. (2020). Explorative study on adaptive façades with superelastic antagonistic actuation, *Struct. Control Health Monit*,*27*:e2463. https://doi.org/10.1002/stc.2463

dos Santos, F. A., Bedon, C., & Sacadura, M., (2016a). Adaptive glass panels using shape-memory alloys. *Glass Struct. Eng.*, *1*, 95–114, DOI 10.1007/s40940-016-0016-3

dos Santos, F. A., Cismasiu, C., & Bedon, C. (2016b). Smart glazed cable façade subjected to a blast loading, *Proceedings of the Institution of Civil Engineers*, *Structures and Buildings*, *169*SB3, 223–232. http://dx.doi.org/10.1680/jstbu.14.00057

dos Santos, F. A., Goncalves, P. F., Cismasiu, C., & Gamboa-Marrufo, M. (2014). Smart glass façade subjected to wind loadings, *Proceedings of the Institution of Civil Engineers, Structures and Buildings*, *167*SB12, 743–752. http://dx.doi.org/10.1680/stbu.13.00011

Elfeki, M. & Youssef, M. (2017). Shape memory alloy reinforced concrete frames vulnerable to strong vertical excitations. *Journal of Building Engineering*, *13*, 272-290.

Gupta, S. (2018a). *Application of shape memory alloy (SMA) material to civil engineering structures*. 1st International Conference on Construction Futures (ICCF), Wolverhampton, UK.

Gupta, S., Morrison, A., Stoddart, E. & Nelson, A. (2018b). *Review of dynamic performance of cladding systems used in blast design.* 1st International Conference on Construction Futures (ICCF), Wolverhampton, UK.

Gupta, S., Stoddart, E. & Morrison, A. (2019). *Use of shape memory alloys to improve structural resilience for extreme load conditions*. SECED conference on Earthquake risk and engineering towards a resilience world, Greenwich, UK, 9-10 September.

ISTECH. (2000*). Shape memory alloy devices for seismic protection of cultural heritage structures.* Proceedings of the final workshop, Ispra, Italy.

Janke, L., Czaderski, C., Motavalli, M., & Ruth, J. (2005). Applications of shape memory alloys in civil engineering structures – overview, limits and new ideas. *Mater Struct*, *38*, 578-592.

Kingery, C.N. & Bulmash, G. (1984). Air blast parameters from TNT spherical air burst and hemispherical surfaces burst. *ARBRL-TR-02555*, Aberdeen Proving Ground, MD: U.S. Army Ballistic Research Laboratory.

Mas, B., Biggs, D., Vieito, I., Cladera, A., Shaw, J., & Martínez-Abella, F. (2017). Superelastic shape memory alloy cables for reinforced concrete applications. *Construction and Building Materials*, *148*, 307-320.

Matthew, S., Speicher, R., DesRoches, R., & Leonb Roberto, T. (2011). Experimental results of a NiTi shape memory alloy (SMA) based re-centering beam-column connection. *Engineering Structures*, *33*, 2448-2457.

Morison, C. (2013). The response of glazing to blast loading. *Engineering and Computational Mechanics*, *166*(EM3), 128-131.

Morison, C. (2007). *The resistance of laminated glass to blast pressure loading and the coefficients for single degree of freedom analysis of laminated glass*. PhD Thesis, Cranfield University.

Nahar, M., Islam, K., & Billah, A.H.M.M. (2020). Seismic collapse safety assessment of concrete beam-column joints reinforced with different types of shape memory alloy rebars. *Journal of Building Engineering*, *29*, 101106.

Piyasena, R.R.C., Thambiratnam, D.P., Chan, T.H.T., & Perera, N.J. (2019). Comparative analysis of blast response of cable truss and cable net façades. *Engineering Failure Analysis*, *104*, 740-757.

Qidwai, M. & Lagoudas D.C. (2000). On thermomechanics and transformation surfaces of polycrystalline NiTi shape memory alloy material. *International Journal of Plasticity*, *16*, 1309-1343.

Royer-Carfagni, G., & Viviani, L. (2020). Basic design of cable-supported glazed surfaces under blast waves. *International Journal of Non-Linear Mechanics*. *123*, 103489.

Shi, G., Fan, H., Bai, Y., & Zheng, J. (2015). Damage evaluation of single-layer cable net façade. *Proceedings of the Institution of Civil Engineers*, *Structures and Buildings*, *168SB3*, 159–173. http://dx.doi.org/10.1680/stbu.13.00006

Song, G., Ma, N., & Li, N.M. (2006). Applications of shape memory alloys in civil structures. *Engineering Structures*, *28*, 1266-1274.

Wang, J., Lia, S., Dezfuli, F.H., & Alam, M.S. (2019). Sensitivity analysis and multi-criteria optimization of SMA cable restrainers for longitudinal seismic protection of isolated simply supported highway bridges. *Structures*, *189*, 509-522.

Yussof, M.M. (2015). *Cable-net supported glass façade systems*. PhD Thesis, University of Surrey.

Zafar, A. & Andrawes, B. (2015). Seismic behaviour of SMA–FRP reinforced concrete frames under sequential seismic hazard. *Engineering Structures*, *98*, 163-173.

Zobec, M., Lori, G., Lumantarna, R., Ngo, T., & Nguyen, C. (2014). Innovative design tool for the optimization of blast-enhanced façade systems. *Journal of Façade Design and Engineering*, *2*, 183-200.